PCCP

Accepted Manuscript

ROYAL SOCIETY OF CHEMISTRY

www.rsc.org/pccp

Proton transfer aiding phase transitions in oxalic acid dihydrate under pressure

Himal Bhatt,[a,*] A. K. Mishra,[a] Chitra Murli,[a] Ashok K. Verma,[a] Nandini Garg,[a] M. N. Deo[a] and Surinder M. Sharma[a]

[a]High Pressure and Synchrotron Radiation Physics Division, Bhabha Atomic Research Centre, Mumbai, 400 085, India

[*] Email: himalphy@gmail.com, hbhatt@barc.gov.in

ABSTRACT. Oxalic acid dihydrate, an important molecular solid in crystal chemistry, ecology and physiology, is being studied for nearly 100 years now. The most debated issues regarding its proton dynamics have arisen due to an unusually short hydrogen bond between the acid and water molecules. Using combined in-situ spectroscopic studies and first-principles simulations at high pressures, we show that the structural modification associated with this hydrogen bond is much more significant than ever assumed. Initially, under pressure, proton migration takes place along this strong hydrogen bond at very low pressures of 2 GPa. This results in the protonation of water with systematic formation of dianionic oxalate and hydronium ion motifs, thus reversing the hydrogen bond hierarchy in the high pressure phase II. The resulting hydrogen bond between hydronium ion and carboxylic group shows remarkable strengthening under pressure, even in the pure ionic phase III. The loss in the cooperativity of hydrogen bonds leads to another phase transition at ~ 9 GPa through reorientation of other hydrogen bonds. The high pressure phase IV is stabilized by a strong hydrogen bond between the dominant CO_2 and H_2O groups of oxalate and hydronium ions respectively. The findings suggest that oxalate systems may provide useful insights on proton transfer reactions and assembly of simple molecules under extreme conditions.

KEYWORDS Oxalic acid dihydrate, Raman scattering, infrared absorption, first principles, Proton transfer, high pressure, Hydronium ion, strong hydrogen bonds

Introduction

Hydrogen bonds play a vital role in the structural stabilization of the fundamental constituents of life such as water and organic acids under varying thermodynamic conditions, such as in planetary interiors and interstellar bodies.[1-7] Strong hydrogen bonds, close to the symmetrization limit, are particularly intriguing due to diverse proton dynamics across the potential barrier under compression.[8] Because of the high barrier in the potential energy, in general, localized proton at the hydrogen bond centre and proton transfer are rare events, as Chandler says 'dynamical bottlenecks'.[9] So far, only in water ice at megabar pressures, the predicted unimodal potential which depicts a symmetric hydrogen bond could be experimentally established using spectroscopy.[10, 11] Crossing the potential barrier, i.e. proton transfer along the hydrogen bond is fundamental to a myriad of physico-chemical and bio-geological processes in nature, for example enzymatic catalysis, signal transduction, acid-base reactions in water gossamers etc.[12-19] Thus, simple carboxylic acid complexes with multiple hydrogen bonds serve as prototypes to study complex processes, which are governed by diverse hydrogen bonding interactions. For example, the cooperativity of hydrogen bonds plays an important role in polypeptide β-sheets and protein folding.[20-22]

Recently, it has been shown that the hidden force responsible for anomalous proton dynamics in O-H---O hydrogen bonds in ice close to symmetrization is the coulombic interaction between covalently shared electron pair and virtually bonded lone pair.[23] Such interactions are enhanced in the cooperative network of several hydrogen bonds in series which eventually increases their strength. For example in Oxalic acid dihydrate $(COOH)_2.2H_2O$, the simplest dicarboxylic acid complex, it results in a very short hydrogen bond O_1-H_t---O_w ($d_{O1\cdots Ow} \sim 2.49$ Å, $\angle O_1HO_w \sim 177^o$) between oxalic acid and water, which makes it an ideal system to study

proton dynamics.[24.] A detailed survey of prior studies on OAD (oxalic acid dihydrate) and some of its applications have recently been reported by Stare and Hadži.[25] In O_1-H_t---O_w, the acceptor O_w (oxygen atom of water) also acts as a donor for the carbonyl group of subsequent OA molecule, forming a chain, –C-O_1-H_t---O_w-H_w---O_2=C-, as shown in Figure 1. The alternate hydrogen bonded chain causes small polarization in the associated bonds, including the covalent ones, thus leading to a net decrease in O---O through the well known cooperativity effect of hydrogen bonds.[25-29] When the hydrogen atom (H_t) moves further towards the bond centre, interesting proton dynamics resulting in increase in anharmonicity and proton migration in the hydrogen bonded network leading to doubly ionized oxalates are expected.

However, the initial beliefs, which date back to 1930s, of observing a proton transfer state of oxalic acid dihydrate at ambient conditions[30-34] was ruled out by a number of x-ray and neutron diffraction and electron density studies which established the presence of neutral oxalic acid with single as well as double C-O bonds.[35-42] Also, at low temperatures only a sustained strengthening of the hydrogen bond was noted.[43-46] The first high pressure powder neutron diffraction experiments up to 0.5 GPa did not show any significant movement in proton.[47] Subsequent studies were primarily focussed on the shortness of this hydrogen bond, where the O---O distance was found to be less than the average carboxylic acid monohydrates as well as the hetero-trimer (with two water molecules) acids.[25, 48-50] The recent DFT calculations by Casati et al. predicted that a proton migrated state may become possible only at pressures as high as 5.3 GPa with the geometry posing a symmetric disposition of hydrogen bond up to this pressure.[51] Their x-ray diffraction studies showed significant changes in molecular geometries, specially the C-O bond lengths, but unambiguous determination of hydrogen atom positions was not possible. The neutron diffraction experiments, carried out on deuterated samples, did not show the proton

migrated state up to 6 GPa, though the accompanied theoretical treatment on neutral and charge transfer configurations provided useful information on this phenomenon.[52] It is the idea, as indicated by theory,[51] of the double minimum on the potential energy surface, with more stable neutral state above 4 GPa, constantly evolving towards the symmetric character up to ~ 5 GPa, that prompted us to look for the possible experimental signatures of hydrogen bond close to the symmetrization limit. Such an event at further higher pressures may bring about equivalence between the constantly competing lone pair and shared bond pair, thereby distorting the cooperativity in hydrogen bonded three dimensional network. Thus, a concerted treatment of the hydrogen bond dynamics and the surrounding cooperative local structure is essential to understand its high pressure behaviour. In this context, spectroscopic studies are the ideal tools as they provide the necessary insights with regard to proton dynamics under pressure.[51]

In the present paper, using infrared (IR) and Raman spectroscopic measurements combined with first-principles simulations on OAD, we provide the first unambiguous experimental evidences of proton migration resulting in a complete transfer of proton from oxalic acid to water at very low pressures (~ 2 GPa). Subsequent to proton transfer, due to the loss of cooperativity of hydrogen bonds, novel high pressure phases, with significant local structure rearrangements, are formed at pressures above 5 GPa.

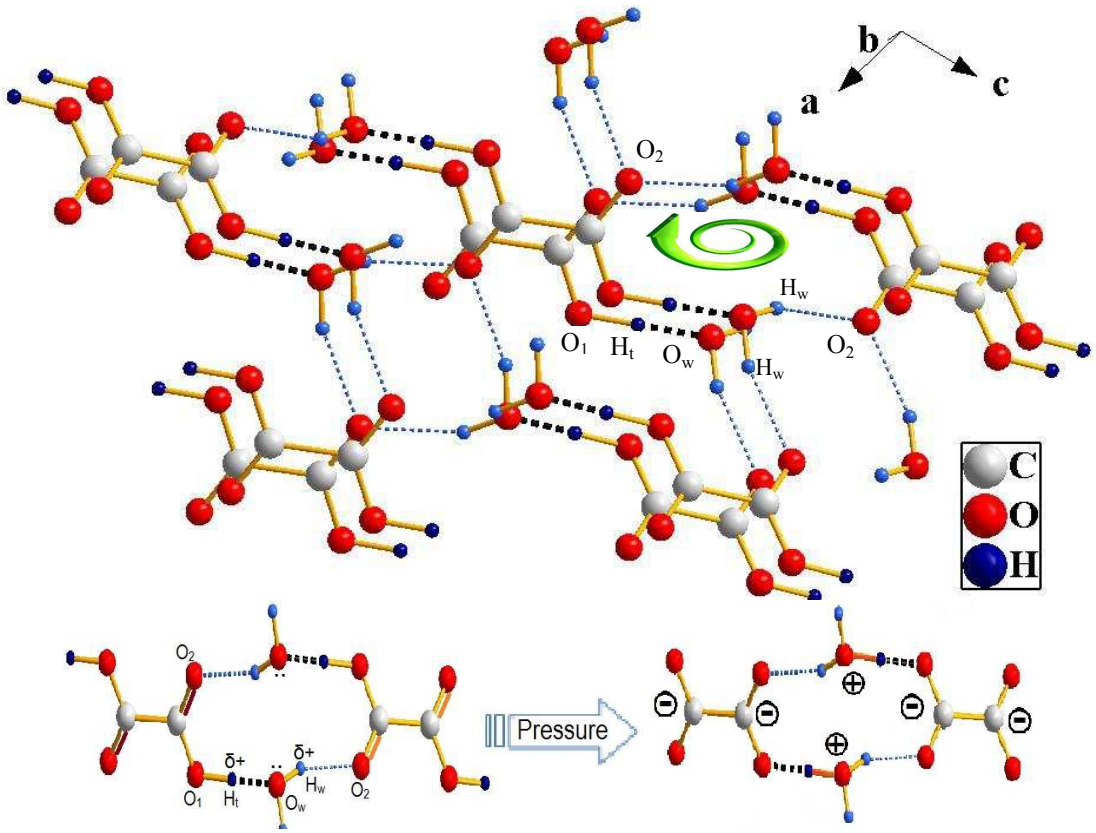

Figure 1. Top: In the three dimensional network in OAD, cooperativity effect among the hydrogen bonds in series runs through spiral motifs along the screw axis to enhance structural stabilization and strengthening of O_1-H_t---O_w hydrogen bond (O_1 and O_2 are single and double bonded oxygen atoms respectively, O_w - water oxygen, H_t - acid hydrogen and H_w - water hydrogen). Here, blue balls and lines (dashed) are hydrogen atoms and bonds respectively and dark blue shows the proton transfer pathway (where water is acceptor). **Bottom:** Two dimensional view of the spiral motif. Pressure induced proton transfer restricts the water oxygen to be an acceptor of hydrogen bond and ionizes the local structural moieties. The higher pressure structure is only tentative.

2. Experimental Details

2.1 Spectroscopic investigations

For infrared studies, an indigenously developed ETH type Diamond Anvil Cell (DAC) was mounted on the sample stage of Hyperion-2000 IR microscope coupled to the Bruker Vertex

80V FTIR spectrometer with a KBr beam splitter and LN_2 cooled HgCdTe detector at IRBL, Inuds-1 facility in India. Powdered sample of α-oxalic acid dihydrate (OAD) (Thomas Baker, 99.99%) dispersed in CsI matrix along with tiny ruby balls of size ~ 5 μm, placed at the center and periphery, was loaded into a 120 μm hole of a tungsten gasket pre-indented to a thickness of ~60 μm. The spectra were recorded at 2 cm^{-1} resolution for clear identification of all the spectral features in the 600 – 4000 cm^{-1} spectral range and repeat measurements were carried out at 4 cm^{-1} resolution. A total of 100 scans were co-added in each case. The observed modes in the background corrected infrared spectra were fitted using a Gaussian profile. The high pressure measurements have been carried out up to 21 GPa with R-lines of ruby fluorescence monitored at each pressure for pressure calibration.[53, 54]

High pressure Raman studies were carried out up to 20 GPa using an indigenously developed confocal micro Raman set up assembled around a HR 460 Jobin Yvon spectrograph equipped with LN_2 cooled Spectrum-One CCD detector. The spectra at each pressure were calibrated using standard neon lines.[53, 54] Polycrystalline sample along with a couple of ~ 5 μm ruby balls were loaded in the pre-indented tungsten gasket of thickness ~70 μm with a hole diameter ~100 μm of a modified Mao-Bell type of DAC. The ambient pressure spectrum of OAD was also recorded using a Bruker MultiRAM FT-Raman spectrometer and all the peak positions were in excellent agreement in the ambient pressure spectra recorded from the two spectrometers.

2.2 Vibrational assignments

α-oxalic acid dihydrate (OAD) is an extensively studied system and its vibrational spectra are well characterized at ambient conditions. The mode assignments in the ambient infrared and Raman spectra have been carried out on the basis of theoretical and experimentally

observed modes of OAD,[24, 55] oxalic acid[56, 57] and various oxalate complexes[8, 57-65] which have also been theoretically verified. To differentiate between various ionic forms of oxalic acid, vibrational studies on neutral-, semi- and dianionic- oxalic acid complexes; and ambient and high pressure infrared and Raman studies on Bis(glycinium)oxalate, and glycinium oxalate were utilized.[8, 58, 62-65] This is supported by simultaneously probing the trend of the high pressure behaviour of IR and Raman active modes of OAD in the present study. Additional information could be retrieved based on the well known vibrational frequencies of hydronium ion.[66-71] For OH stretching modes, the correlation curves for stretching frequencies as a function of hydrogen bond strength, i.e. bond parameters have also been used.[72, 73]

2.3 First Principles DFT calculations

The first-principles structural relaxations, as a function of volume, were carried out using Vienna ab-initio Simulation Package (VASP computer code) in order to corroborate our experimental results on proton transfer.[74-77] The initial structure model was constructed on the basis of reported experimental data.[51, 78] The exchange-correlation functional was treated with the generalized gradient corrected scheme of Perdew-Burke-Ernzerhof (PBE).[79] The interactions between valence electrons and core were treated within the frozen-core all electron projector-augmented-wave (PAW) approach. Plane wave basis set was constructed using 600 eV energy cut off and the full Brillouin zone was sampled using a uniform 6×12×4 Monkhorst-Pack k point mesh.[80] Cell shape and ions positions were optimized as a function of cell volume. Pressure corresponding to a given cell volume was read from the output file of code. Figure 2 displays the calculated crystal structures of OAD at ambient pressure and 1.5 GPa. As the crystal structures of the high pressure phases subsequent to proton transfer (above 2 GPa) were not known, the computational treatment has not been extended to higher pressures.

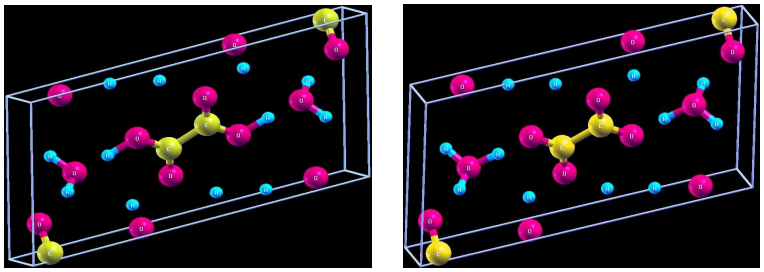

Figure 2. Simulated crystal structure of α-oxalic acid dihydrate (monoclinic, $P2_1/n$) at (a) 0.1 MPa, (b) 1.5 GPa. Thermal ellipsoids are shown at the 50% probability level; yellow, red and cyan balls denote C, O and H atoms respectively.

3. Results and Discussion

The hydrogen bonds connecting the acid groups of oxalic acid to the two water molecules on both sides are close to the symmetrization limit in OAD. In such strong O-H---O hydrogen bonds, the proton is relatively delocalized and the virtual bond has small covalent character.[23] The delocalization of proton results in interactions of the νOH (stretching) mode with other bridge vibrations and crystal modes.[81, 82] This leads to a broad absorption band, resembling a continuum, in the infrared spectrum.[83-87] The centre of this band has been reported at nearly 2100 cm^{-1} for oxalic acid dihydrate.[24, 25] If the hydrogen bond further strengthens under pressure and progresses towards a symmetric state, as predicted by theory,[51] the νOH mode is expected to show softening accompanied with dampening. This would lead to an increase in system anharmonicity resulting in cascading interactions between vibrational energy levels.[11] However, depending upon the barrier height of the double well potential, any external stimuli may also result in the reorientation of hydrogen bond or immediate crossing over of the potential barrier. In the latter case of proton migration along O_1-H_t---O_w, one would expect protonation of water thus forming hydronium ion. The present work provides key spectroscopic evidences of this phenomenon as described below.

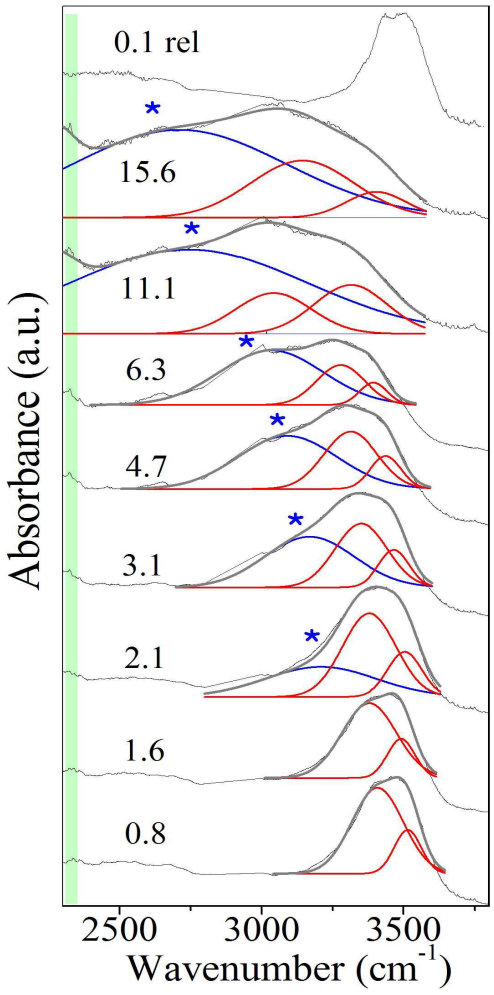

Figure 3. High pressure infrared spectra of OAD in the region 2300 – 3800 cm^{-1} which shows evolution of the water stretching region with pressure; here asterisks (*) show the emergence of H_3O^+ stretching band (blue) with pressure and the spectra are normalized with respect to instrumental and environmental effects. Light green shaded bar is the diamond absorption region and numbers denote pressure values in GPa ('rel' - release).

In Figure 3, the vibrational stretching region (3250 – 3600 cm^{-1}) corresponding to the water O_w-H_w bonds has been shown which depicts two clear bands in the ambient phase. At high pressures, above 2 GPa, we note the emergence of the characteristic ν_1 (O_w-H_t) IR mode at ~ 3100 cm^{-1} which confirms the formation of hydronium ion (H_3O^+),[70, 71] thus implying

protonation of water molecules across 2 GPa in oxalic acid dihydrate. In the corresponding pressure range, proton migration from oxalic acid molecules is also revealed by an abrupt non-discernibility of the spectral signatures of oxalate O_1-H_t bond (Figure 4), i.e. the broad stretching band, deformation modes as well as the features due to νOH mode couplings like the Evans transmission window (a relatively sharper negative dip near 1800 cm^{-1}, denoted by ♦).[24] These observations are well supported by the theoretical calculations that the proton transfer along O_1-H_t---O_w takes place at quite low pressures (Figure 2), which is indicated by a reversal in the bond parameters of O_1-H_t (d_{OH}: ambient - 1.161 Å, 1.5 GPa - 1.30 Å) and H_t---O_w (d_{HO}: ambient - 1.267 Å, 1.5 GPa - 1.14 Å) bonds above 1.5 GPa. Different results in an earlier computational study may be due to a different computational methodology.[51]

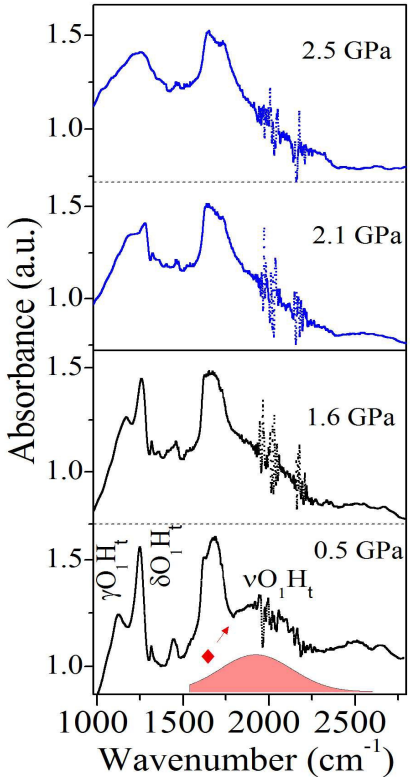

Figure 4. Mid infrared spectra of OAD in range 1000 – 2800 cm^{-1} up to 2.5 GPa, before (black) and after (blue) the proton transfer. Here an arbitrarily drawn band (shaded pink) is shown to mark the presence of

a broad absorption related to νOH mode at ambient conditions, small fluctuations near 2000 cm^{-1} are due to second order diamond absorption and '♦' (in red) denotes the reported Evans transmission dip for OAD.[24]

While the emergence of hydronium ν_1 mode indicates protonation of water, its width indicates formation of another hydrogen bond suggesting reversal of hydrogen bond hierarchy. The position of this mode, i.e. a relatively higher frequency, indicates asymmetrization of the resulting hydrogen bond, as also predicted by the calculated bond parameters $d_{O\text{-}H}$ and $d_{H\text{---}O}$. The stiffening of the $\nu O_1\text{---}O_w$ Raman mode (~ 280 cm^{-1})[24, 88] up to 2 GPa (Figure 5c) and softening thereafter up to 5 GPa provides experimental evidence of the elongation of $O_1\text{---}O_w$ upon proton transfer (see also Table 1). In the subsequent sections, we discuss the molecular structure, mechanism of this proton transfer and the resulting hydrogen bonded network through the study of vibrational modes corresponding to COOH and OH groups of oxalate and water motifs respectively.

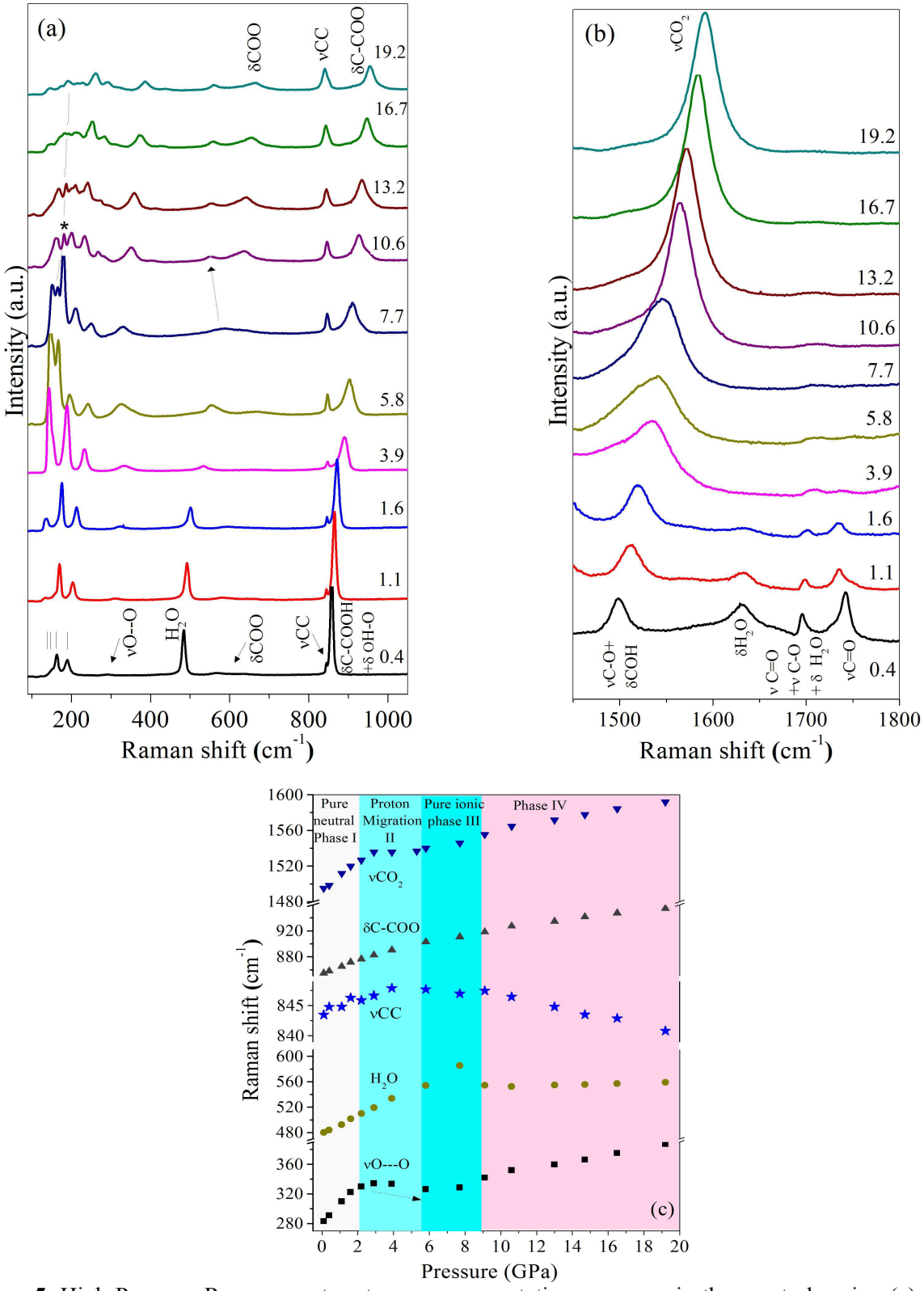

Figure 5. High Pressure Raman spectra at some representative pressures in the spectral region (a) 90 – 1050 cm^{-1} and (b) 1450 – 1800 cm^{-1}; the spectra, plotted in the same intensity scale, have been offset for

clarity in both the regions; numbers are pressure values in GPa (c) Variation of some important Raman modes with pressure.

3.1. Changes observed in the oxalate motifs

In oxalic acid, while the migration of proton (H_t) is revealed by the systematic vanishing of the intense O_1H_t deformation IR modes, i.e. out of plane (γO_1H_t ~1145 cm^{-1}) and in-plane (δO_1H_t coupled to νC-O ~1255 cm^{-1}) bending modes, with pressure (Figures 4 and 6), the transition to ionic state above 2 GPa due to loss of proton is indicated by the emergence of a new, relatively sharper, νC-O IR mode near 1318 cm^{-1} (Figure 6) which is a characteristic mode of dianionic form of oxalate (devoid of any hydrogen) and its relative intensity increases with pressure.[58, 62] It is noteworthy that the neutral state of oxalic acid in OAD is characterized by strong coupling between various modes.[24] For example, the C-O (ν_{asy}: 1621 cm^{-1}) and C=O (~1680 cm^{-1}) bond stretching vibrational energy levels are strongly coupled, which has been attributed to Fermi resonance.[55, 56] This coupling results in a complex spectral profile near 1700 cm^{-1} and is expected to push the energy levels apart at ambient conditions. Under compression, systematic vanishing of this coupling is revealed by the large stiffening and softening in the ν_{asy}C-O and νC=O IR modes respectively which brings the two modes closer, as shown in Figure 7a. Eventually, the disappearance of the C=O signature is complete and only a single broad band, resembling the CO_2 asymmetric stretching mode of dianionic oxalate is observed (Figure 6) in the ionic phase III above ~ 5 GPa.[58] The vanishing of νC=O features in the 1700 cm^{-1} region, as also clearly evident in the Raman spectra beyond 2 GPa (Figure 5b) is a definite signature of loss in the double bond character and emergence of anionic form of oxalate on both the carboxyl sides. This implies an equivalence of the two CO bonds in the acid group. The bond parameters obtained from first principles calculations have also shown that C-O (1.284 Å (at 0.1 MPa),

1.269 Å (at 1.5 GPa)) and C=O (1.251 Å (at 0.1 MPa), 1.261 Å (at 1.5 GPa)) bond lengths in OA approach each other upon proton migration. Thus, as the proton is transferred from oxalate carboxyl group to water at ~ 2 GPa, all the C-O bonds in the COOH groups, in high pressure phase II, systematically become equivalent up to nearly 5 GPa, above which they are essentially indistinguishable in phase III (Table 1). The above spectroscopic observations also qualitatively explain the geometrical modifications in the C-O bonds measured earlier using x-ray diffraction.[51]

The changes observed in the CO_2 deformation region (600 – 800 cm^{-1}) in high pressure IR spectra (Figure 6) upon proton (H_t) transfer are also consistent with the above observations. While the $\delta CCOOH_t$ mode (~ 620 cm^{-1}),[24] which weakens under pressure, merges with a new mode appeared near 715 cm^{-1} at 2.1 GPa and systematically transform in to the δCO_2 band of dianionic oxalate,[58] the (δCO_2 + δOH_w) coupled mode[24] near 725 cm^{-1} shows a discontinuous jump across 2 GPa (Figure 7b) suggesting an abrupt change in the electronic environment of acid $COOH_t$ and water OH_w groups across 2 GPa.

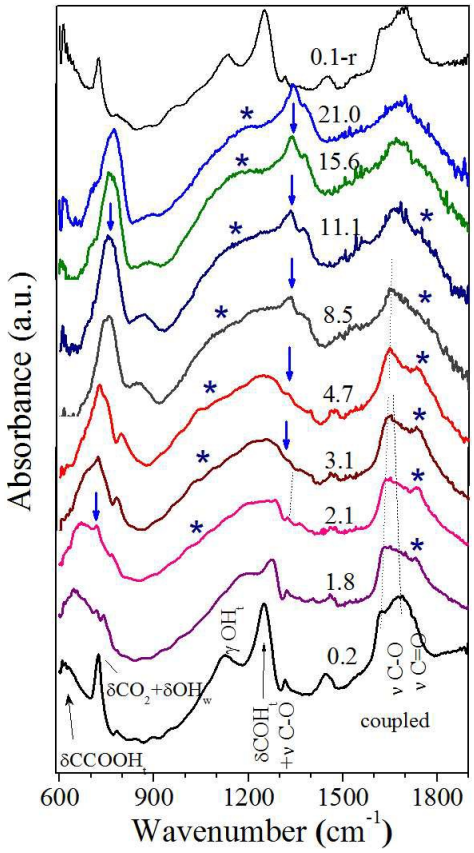

Figure 6. High pressure infrared spectra of OAD in the range 600 – 1850 cm^{-1}. Here asterisks (*) show H_3O^+ features and blue down arrows show dianionic oxalate features emerging with pressure and 'r' denotes data on release. Numbers denote pressure values in GPa.

3.3. Changes observed in the water motifs

The structural arrangement in hydronium ion, and other similar structures like ammonia, is distinguished by their characteristic deformation modes. The weak shoulder in δH_2O IR mode coupled with νC=O (~ 1726 cm^{-1}) also shows a discontinuous increase in position and width above 2 GPa due to simultaneous change in the C=O and H_2O electronic environment upon proton transfer and the mode observed beyond 2 GPa is therefore attributed to the ν_4 mode of H_3O^+ (Figures 6 and 7a). Note that the ν_4 mode of H_3O^+ (found in the range 1670 – 1750 cm^{-1}) is

observed at a higher frequency than the ν_2 mode of H_2O (1596 – 1700 cm^{-1}).[70] For the hydronium ion, ν_2 deformation mode, based on the umbrella inversion motion, is expected in the range 1000 – 1200 cm^{-1}.[66-70] We distinctly see the evolution of this mode in the IR spectra (Figure 6) around ~ 1020 cm^{-1} across 2 GPa, beyond which it systematically gains intensity and stiffens with pressure (Figure 7b and Table 1). The first-principles calculations also indicate that ∠HOH, around 105.8° at ambient conditions, shows an increase at 1.5 GPa and the three angles in the protonated phase become ~ 107°, 112° and 115°, in reasonable accord with the hydronium structure.[89] The above spectroscopic and theoretical observations are also accompanied with vanishing of the δH_2O coupled Raman mode (~ 1630 cm^{-1}) at 2 GPa (Figure 5b).

Noticeably, the O-H_w bonds of water get elongated under compression as indicated by the softening behaviour of νO-H_w IR modes with pressure (Figure 7a). This behavior is well supported by the calculated bond parameters, i.e. the two $d_{O\text{-}H}$ distances of water (0.996 Å and 0.997 Å) which show an increase (1.009 Å and 1.014 Å) and become comparable with the O_w-H_t distance (1.14 Å, bond formed after the proton transfer) under pressure. Indeed, the cooperative mechanism favors such an elongation and strengthening of the corresponding hydrogen bonds. However, we observe continued softening of all the three νOH modes in the hydronium structure even after the proton transfer indicating strengthening of all the O-H---O interactions. The most interesting feature of the incipient (phase II, above 2 GPa) and pure ionic phase (III, above 5 GPa) is the remarkable pressure induced broadening (Figure 3) accompanied by a large rate of softening (> 50 cm^{-1}/GPa) (Figure 7a and Table 1) of the newly emerged νO_w-H_t hydronium mode (ν_1) indicating increase in anharmonicity. We also notice that the νO_1--O_w Raman mode shows stiffening above 5 GPa (Figure 5c and Table 1). Therefore it is anticipated that this hydrogen bond, between -CO_2^- and H_3O^+ groups may be strengthened to the symmetrization

limit at very high pressures. The pressure induced behavior of the νO_w-H_t hydronium mode shown in Figure 7a, in the range 2 to 9 GPa, could be well approximated by the formula $\nu = [A(P_c\text{-}P)]^{1/2}$, which predicts $P_c \sim 36$ GPa as the pressure corresponding to νOH mode instability.[90] However, the rate of νOH_t softening, depicting the power law behaviour analogous to the soft mode, reduces above 9 GPa, indicating another structural modification across this pressure.

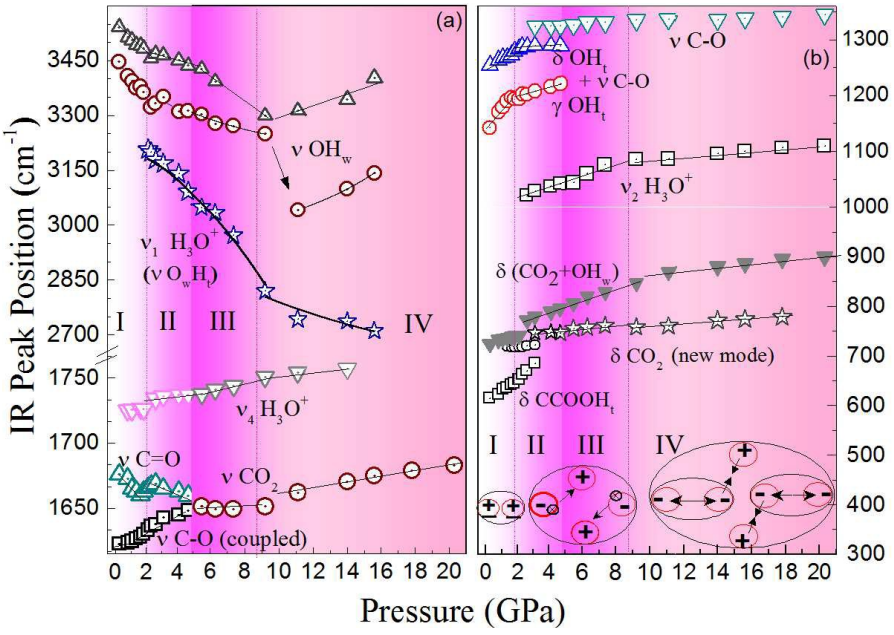

Figure 7. Pressure induced variation of infrared active modes ((a) 1600 – 3600 cm^{-1}, (b) 600 – 1350 cm^{-1}) of OAD in the ambient phase I, proton transfer phase II, ionic phase III and the high pressure phase IV above 9 GPa (shown by a cartoon in b).

4. Proton transfer aided phase transition

In OAD (monoclinic structure, space group $P2_1/n$), a layered spiral structure of oxalic acid and water molecules is formed along the screw axis due to excess stabilization of hydrogen bonds resulting from their cooperative behaviour (Figure 1, top). Subsequent to proton transfer,

the hydronium oxygen is no more a hydrogen bond acceptor (Figure 1, bottom). But, the sustained strengthening of all the O-H---O interactions, as discussed above, may imply continued elongation of hydronium O-H bond lengths. It is only across 9 GPa that the νOH_w frequency variations show discontinuous behaviour and they start stiffening thereafter (Figure 7a), suggesting loss of cooperativity. Across 9 GPa, we also observe the emergence of new Raman modes in the lattice region (Figure 5a) and slope change in the frequency versus pressure plots of many IR and Raman modes (Table 1).

These results point towards a phase transition in OAD at 9 GPa. Across the transition, the water libration Raman mode (~ 480 cm^{-1}),[24] which showed monotonous stiffening and broadening upon proton transfer (Figure 5c), also displays a discontinuous jump and slope change. Therefore, the abrupt shift of the νO_w-H_w mode across 9 GPa (Figure 7a) can also be linked to breaking and reformation of the relatively weaker O_w-H_w---O_2 hydrogen bonds. On the other hand, the νO_w-H_t mode continues to soften in the high pressure phase IV above 9 GPa, though at a lesser rate, with increase in width up to the highest pressure measured, i.e. 21 GPa. This is also accompanied with monotonous stiffening of the νO_1---O_w Raman mode (O_1---H_t-O_w) as observed from Figure 5c, which indicates sustained strengthening of this hydrogen bond in phase IV above 9 GPa.

Such a hydrogen bond strengthening may however pull the oxalate motif from both sides thus squeezing the spiral motif (Figure 1 top), which gets support from the repulsion between the resonating electronic densities in the two COO^- ends of oxalate ion due to loss of proton (see also the cartoon in Figure 7b). But this squeezing is limited by the stiff C-C backbone of oxalate molecule. We observe that in the new phase above 9 GPa, the νCC Raman mode is found to soften with pressure up to the highest pressure recorded in this study, i.e. 20 GPa, and the rate of

this softening (~ 0.8 cm^{-1}/GPa) is significant in view of the strength of this bond (Figure 5c), thus weakening the backbone. The νCO_2 Raman mode near 1500 cm^{-1} also shows pronounced stiffening accompanied with steep rise in the relative intensity (Figure 5b).

Therefore, one may expect that the O_1---H_t-O_w hydrogen bond, between the dominant CO_2 and H_3O^+ groups gains significant strength at high pressures, and, if it continues to strengthen at further higher pressures, would lead to a structure with the two fundamental entities, CO_2 and H_2O hinging through a proton. It would be interesting to look for the resulting structural arrangement and hydrogen position at very high pressures above 20 GPa. These results would be helpful in understanding the structural assembly of simple molecules under extreme thermodynamic conditions prevailing in primitive earth, planetary interiors or extra-terrestrial systems.

Conclusions

To summarize, we have reported the first experimental evidences of a complete proton transfer in oxalic acid dihydrate, the simplest dicarboxylic acid complex, at moderate pressures of 2 GPa. The influence of this phenomenon on the three dimensional hydrogen bonded network and local molecular structures has been studied. Distinctive signatures of a systematic transition from neutral to doubly ionized species of oxalic acid and the formation of hydronium ion, which acts as a donor to three hydrogen bonds in the subsequent high pressure phases above 2 GPa, has been confirmed. As a result, there is a loss in the cooperativity of hydrogen bonds leading to another phase transition across 9 GPa through reorientation of hydrogen bonds. The high pressure spectroscopic results further suggest that, subsequent to transfer, the proton again moves

in the reverse direction, thus significantly strengthening the new hydrogen bond between the dominant CO_2 and H_3O groups, up to the highest pressure measured, i.e. 21 GPa.

These observations on proton dynamics are interesting from the point of view of two important fundamental problems. First the 'transport mechanism of hydrated proton', crucial for molecular theories of ionic systems and interstellar research, and second, understanding 'proton transfer pathways in protein environments', important to study protein-protein interactions and enzymatic catalysis. Indeed, the high pressure behaviour of hydronium ion, the simplest oxonium ion is of immense relevance in acid-base reactions and mineralogy. Thus simple oxalate complexes, in various ionic forms, with remarkable sensitivity to pressure tuning at moderate pressures can be exploited as archetype systems to study proton dynamics in various bio-geological processes.

References

1 A. Aubrey, H. J. Cleaves, J. H. Chalmers, A. M. Skelley, R. A. Mathies, F. J. Grunthaner, P. Ehrenfreund and J. L. Bada, *Geology*, 2006, **34**, 357-360.

2 M. P. Bernstein, J. P. Dworkin, S. A. Sandford, G. W. Cooper and L. J. Allamandola, *Nature*, 2002, **416**, 401-403.

3 A. Brack and C. T. Pillinger, *Extremophiles*, 1998, **2**, 313-319.

4 P. A. Gerakines and R. L. Hudson, *Astrobiology*, 2013, **13**, 647-655.

5 T. Otake, T. Taniguchi, Y. Furukawa, F. Kawamura, H. Nakazawa and T. Kakegawa, *Astrobiology*, 2011, **11**, 799-813.

6 A. Sharma, J. H. Scott, G. D. Cody, M. L. Fogel, R. M. Hazen, R. J. Hemley and W. T. Huntress, *Science*, 2002, **295**, 1514-1516.

7 A. Witze, *Nature*, 2015, **523**, 389–390.

8 H. Bhatt, C. Murli, A. K. Mishra, A. K. Verma, N. Garg, M. N. Deo, R. Chitra and S. M. Sharma, *J. Phys. Chem. B*, 2016, **120**, 851-859.

9 D. Chandler, *Classical and Quantum Dynamics in Condensed Phase Simulations,*, edited by B. J. Berne, G. Ciccotti and D. F. Coker (World Scientific, Singapore) 1998, 3.

10 M. Benoit, D. Marx and M. Parrinello, *Nature*, 1998, **392**, 258-261.

11 V. V. Struzhkin, A. F. Goncharov, R. J. Hemley and H.-k. Mao, *Phys. Rev. Lett.*, 1997, **78**, 4446-4449.

12 D. Antoniou, S. Caratzoulas, C. Kalyanaraman, J. S. Mincer and S. D. Schwartz, *Europ. J. Biochem.*, 2002, **269**, 3103-3112.

13 T. C. Berkelbach, H.-S. Lee and M. E. Tuckerman, *Phys. Rev. Lett.*, 2009, **103**, 238302.

14 A. Hassanali, F. Giberti, J. Cuny, T. D. Kühne and M. Parrinello, *Proc. Nat. Acad. Sc.*, 2013, **110**, 13723-13728.

15 M. Heyden and D. J. Tobias, *Phys. Rev. Lett.*, 2013, **111**, 218101 (218101-218105).

16 H. Ishikita and K. Saito, *J. Royal Soc. Interface*, 2014, **11**, 20130518 (20130511-20130517).

17 A. Kohen, R. Cannio, S. Bartolucci and J. P. Klinman, *Nature*, 1999, **399**, 496-499.

18 P. A. Sigala, A. T. Fafarman, J. P. Schwans, S. D. Fried, T. D. Fenn, J. M. M. Caaveiro, B. Pybus, D. Ringe, G. A. Petsko, S. G. Boxer and D. Herschlag, *Proc. Nat. Acad. Sc.*, 2013, **110**, E2552-E2561.

19 C. A. Wraight, *Biochim. Biophys. Acta*, 2006, **1757**, 886-912.

20 N. Kobko and J. J. Dannenberg, *J. Phys. Chem. A*, 2003, **107**, 10389-10395.

21 N. Kobko, L. Paraskevas, E. del Rio and J. J. Dannenberg, *J. Am. Chem. Soc.*, 2001, **123**, 4348-4349.

22 G. Rossetti, A. Magistrato, A. Pastore and P. Carloni, *J. Chem. Th. Comput.*, 2010, **6**, 1777-1782.

23 C. Q. Sun, X. Zhang and W. Zheng, *Chem. Sc.*, 2012, **3**, 1455-1460.

24 V. Mohaček-Grošev, J. Grdadolnik, J. Stare and D. Hadži, *J. Ram. Spec.*, 2009, **40**, 1605-1614.

25 J. Stare and D. Hadži, *J. Chem. Th. Comput.*, 2014, **10**, 1817-1823.

26 T. Steiner, B. Lutz, J. van der Maas, N. Veldman, A. M. M. Schreurs, J. Kroon and J. A. Kanters, *Chem. Commun.*, 1997, 191-192.

27 G. A. Jeffrey and W. Saenger, *Hydrogen Bonding in Biological Structures, Springer, Berlin*, 1991.

28 G. A. Jeffrey, *An Introduction to Hydrogen Bonding; Oxford University Press: New York*, 1997.

29 T. Steiner, *Cryst. Rev.*, 1996, **6**, 1-51.

30 A. D. Booth, *Proc. Royal Soc. Lond. A: Math. Phys. Eng. Sc.*, 1947, **190**, 490-496.

31 R. Brill, C. Hermann and C. Peters, *Annal. der Phys.*, 1943, **434**, 357-377.

32 J. D. Dunitz and J. M. Robertson, *J. Chem. Soc.*, 1947, 142-148.

33 J. M. Robertson and A. R. Ubbelohde, *Proc. Royal Soc. Lond. A: Math. Phys. Eng. Sc.*, 1939, **170**, 222-240.

34 J. M. Robertson and I. Woodward, *J. Chem. Soc.*, 1936, 1817-1824.

35 F. R. Ahmed and D. W. J. Cruickshank, *Acta Cryst.*, 1953, **6**, 385-392.

36 P. Coppens and T. M. Sabine, *Acta Cryst.*, 1969, **B25**, 2442-2451.

37 P. Coppens, T. M. Sabine, G. Delaplane and J. A. Ibers, *Acta Cryst.*, 1969, **B25**, 2451-2458.

38 J. Dam, S. Harkema and D. Feil, *Acta Cryst.*, 1983, **B39**, 760-768.

39 A. Lehmann, P. Luger, C. W. Lehmann and R. M. Ibberson, *Acta Cryst.*, 1994, **B50**, 344-348.

40 T. M. Sabine, G. W. Cox and B. M. Craven, *Acta Cryst.*, 1969, **B25**, 2437-2441.

41 E. D. Stevens and P. Coppens, *Acta Cryst.*, 1980, **B36**, 1864-1876.

42 E. D. Stevens, P. Coppens, R. Feld and M. S. Lehmann, *Chem. Phys. Lett.*, 1979, **67**, 541-543.

43 A. Levstik, C. Filipič, V. Bobnar, I. Levstik and D. Hadži, *Phys. Rev. B*, 2006, **74**, 153104.

44 A. Martin and A. A. Pinkerton, *Acta Cryst.*, 1998, **B54**, 471-477.

45 Y. Wang, C. J. Tsai, W. L. Liu and L. D. Calvert, *Acta Cryst.*, 1985, **B41**, 131-135.

46 D. Zobel, P. Luger, W. Dreissig and T. Koritsanszky, *Acta Cryst.*, 1992, **B48**, 837-848.

47 M.-L. Putkonen, R. Feld, C. Vettier and M. S. Lehmann, *Acta Cryst.*, 1985, **B41**, 77-79.

48 T. Steiner, *Angewandte Chemie International Edition*, 2002, **41**, 48-76.

49 P. Vishweshwar, N. Jagadeesh Babu, A. Nangia, S. A. Mason, H. Puschmann, R. Mondal and J. A. K. Howard, *J. Phys. Chem. A*, 2004, **108**, 9406-9416.

50 P. Vishweshwar, A. Nangia and V. M. Lynch, *Chem. Commun.*, 2001, 179-180.

51 N. Casati, P. Macchi and A. Sironi, *Chem. Commun.*, 2009, 2679-2681.

52 P. Macchi, N. Casati, W. G. Marshall and A. Sironi, *CrystEngComm*, 2010, **12**, 2596-2603.

53 A. Dewaele, P. Loubeyre and M. Mezouar, *Phys. Rev. B*, 2004, **70**, 094112.

54 G. J. Piermarini, S. Block, J. D. Barnett and R. A. Forman, *J. Appl. Phys.*, 1975, **46**, 2774-2780.

55 Y. Ebisuzaki and S. M. Angel, *J. Ram. Spec.*, 1981, **11**, 306-311.

56 J. de Villepin and A. Novak, *Spectrochim. Acta A: Mol. Spec.*, 1978, **34**, 1009-1017.

57 J. de Villepin, A. Novak and D. Bougeard, *Chem. Phys.*, 1982, **73**, 291-312.

58 H. Bhatt, C. Murli, N. Garg, M. N. Deo, R. Chitra, R. R. Choudhury and S. M. Sharma, *Chem. Phys. Lett.*, 2012, **532**, 57-62.

59 J. de Villepin and A. Novak, *Spectroscopy Lett.*, 1971, **4**, 1-8.

60 J. de Villepin and A. Novak, *J. Mol. Str.*, 1976, **30**, 255-269.

61 D. Hadži and B. Orel, *J. Mol. Struc.*, 1973, **18**, 227-239.

62 Y. M. Jung, *Bull. Korean Chem. Soc.*, 2003, **24**, 1410-1412.

63 A. K. Mishra, C. Murli, H. Bhatt and S. M. Sharma, *AIP Conf. Proc.*, 2014, **1591**, 136-138.

64 A. K. Mishra, C. Murli, N. Garg, R. Chitra and S. M. Sharma, *J. Phy. Chem. B*, 2010, **114**, 17084-17091.

65 D. Sajan, J. Binoy, B. Pradeep, K. Venkata Krishna, V. B. Kartha, I. H. Joe and V. S. Jayakumar, *Spectrochim. Acta A: Mol. Biomol. Spec.*, 2004, **60**, 173-180.

66 D. E. Bethell and N. Sheppard, *J. Chem. Phys.*, 1953, **21**, 1421-1421.

67 C. C. Ferriso and D. F. Horning, *J. Am. Chem. Soc.*, 1953, **75**, 4113-4114.

68 P. A. Giguère and S. Turrell, *Canad. J. Chem.*, 1976, **54**, 3477-3482.

69 N. N. Haese and T. Oka, *J. Chem. Phys.*, 1984, **80**, 572-573.

70 R. W. T. Wilkins, A. Mateen and G. W. West, *Am. Mineralog.*, 1974, **59**, 811-819.

71 G. V. Yukhnevich, *Russ. Chem. Rev.*, 1963, **32**, 619-633.

72 K. Nakamoto, M. Margoshes and R. E. Rundle, *J. Am. Chem. Soc.*, 1955, **77**, 6480-6486.

73 S. K. Sikka, *High Press. Res.*, 2007, **27**, 313-319.

74 P. E. Blöchl, *Phys. Rev. B*, 1994, **50**, 17953-17979.

75 G. Kresse and J. Furthmüller, *Comput. Mat. Sc.*, 1996, **6**, 15-50.

76 G. Kresse and J. Hafner, *J. Phys.: Cond. Mat.*, 1994, **6**, 8245-8257.

77 G. Kresse and D. Joubert, *Phys. Rev. B*, 1999, **59**, 1758-1775.

78 R. G. Delaplane and J. A. Ibers, *Acta Cryst.*, 1969, **B25**, 2423-2437.

79 J. P. Perdew, K. Burke and M. Ernzerhof, *Phys. Rev. Lett.*, 1996, **77**, 3865-3868.

80 H. J. Monkhorst and J. D. Pack, *Phys. Rev. B*, 1976, **13**, 5188-5192.

81 N. Huse, K. Heyne, J. Dreyer, E. T. J. Nibbering and T. Elsaesser, *Phys. Rev. Lett.*, 2003, **91**, 197401.

82 J. Stare, J. Panek, J. Eckert, J. Grdadolnik, J. Mavri and D. Hadži, *J. Phys. Chem. A*, 2008, **112**, 1576-1586.

83 R. Janoschek, E. G. Weidemann, H. Pfeiffer and G. Zundel, *J. Am. Chem. Soc.*, 1972, **94**, 2387-2396.

84 R. Janoschek, E. G. Weidemann and G. Zundel, *J. Chem. Soc., Far. Trans. 2: Mol. Chem. Phys.*, 1973, **69**, 505-520.

85 T. Lankau and C.-H. Yu, *Phys. Chem. Chem. Phys.*, 2011, **13**, 12758-12769.

86 L. Sobczyk, *Mol. Phys. Rep.*, 1996, **14**, 19-31.

87 G. Zundel, *J. Mol. Struc.*, 2000, **552**, 81-86.

88 Y. Huang, X. Zhang, Z. Ma, Y. Zhou, W. Zheng, J. Zhou and C. Q. Sun, *Coord. Chem. Rev.*, 2015, **285**, 109-165.

89 P. A. Kollman and C. F. Bender, *Chem. Phys. Lett.*, 1973, **21**, 271-274.

90 A. F. Goncharov, M. R. Manaa, J. M. Zaug, R. H. Gee, L. E. Fried and W. B. Montgomery, *Phys. Rev. Lett.*, 2005, **94**, 065505.

Table 1. A summary of changes observed in the vibrational modes in various high pressure phases. A negative slope indicates pressure induced softening.

Vibrational mode	Value at 0.1 MPa (cm^{-1})	Slope (dv/dP) cm^{-1}/GPa				Remarks
		Atm–2 GPa Phase I	2–5 GPa Phase II	5 – 9 GPa Phase III	> 9 GPa Phase IV	
Raman						
νO_1---O_w	282	22.2	- 3.05	4.71	4.49	
lib. H_2O	480	14.22	12.16	16.1	0.43	Discontinuous shift across 9 GPa
νCC	846	1.14	0.5	0.06	-0.76	
νCO_2	1493	15.03	1.5	4.9	3.6	Intensity increases above 5 and 9 GPa
δH_2O coupled mode	1630	1.4				Vanishes above 2 GPa
νC=O	1740	-5.05	weak			Vanishes above 2 GPa
νCO+νC=O+ δOH	1694	3.4	weak	weak	weak	
IR						
νC=O	1680	-5.3	-2.3	0.05	2.8	Merge into a band above 5 GPa
νCO+νC=O+ δOH	1621	5.6	4.9			
νC-O			1.04	2.4	1.25	
δOH+ νC-O	1255	15.4	5.9			Vanishes above 5 GPa
γOH	1145	27.5	10.5			Vanishes above 5 GPa
νOH water	3540 3448	-52.1 -36.2	- 4.5 - 8.3	- 14.5 - 34.5	22.4 16.15	Discontinuous shift across 9 GPa
$\nu_1 H_3O^+$			- 45.9	- 60.4	- 7.5	
$\nu_2 H_3O^+$			10	2.3	1.3	
$\nu_4 H_3O^+$			1.43	3.0	1.32	
δ (CO_2+H_2O)	725	6.05	11.5	10.9	3.2	Discontinuous shift across 2 GPa